A Terrestrial-mass Rogue Planet Candidate Detected in the Shortest-timescale Microlensing Event

Przemek Mróz[1,2] ⓘ, Radosław Poleski[2] ⓘ, Andrew Gould[3,4], Andrzej Udalski[2] ⓘ, Takahiro Sumi[5]
and
Michał K. Szymański[2] ⓘ, Igor Soszyński[2] ⓘ, Paweł Pietrukowicz[2] ⓘ, Szymon Kozłowski[2] ⓘ, Jan Skowron[2] ⓘ,
Krzysztof Ulaczyk[2,6] ⓘ
(OGLE Collaboration),
and
Michael D. Albrow[7] ⓘ, Sun-Ju Chung[8,9] ⓘ, Cheongho Han[10], Kyu-Ha Hwang[8] ⓘ, Youn Kil Jung[8], Hyoun-Woo Kim[8],
Yoon-Hyun Ryu[8] ⓘ, In-Gu Shin[8] ⓘ, Yossi Shvartzvald[11] ⓘ, Jennifer C. Yee[12] ⓘ, Weicheng Zang[13] ⓘ, Sang-Mok Cha[8,14],
Dong-Jin Kim[8], Seung-Lee Kim[8,9], Chung-Uk Lee[8], Dong-Joo Lee[8], Yongseok Lee[8,14], Byeong-Gon Park[8,9], and
Richard W. Pogge[4] ⓘ
(KMT Collaboration)
[1] Division of Physics, Mathematics, and Astronomy, California Institute of Technology, Pasadena, CA 91125, USA; pmroz@astro.caltech.edu
[2] Astronomical Observatory, University of Warsaw, Al. Ujazdowskie 4, 00-478 Warszawa, Poland
[3] Max Planck Institute for Astronomy, Königstuhl 17, D-69117 Heidelberg, Germany
[4] Department of Astronomy, Ohio State University, 140 W. 18th Avenue, Columbus, OH 43210, USA
[5] Department of Earth and Space Science, Graduate School of Science, Osaka University, Toyonaka, Osaka 560-0043, Japan
[6] Department of Physics, University of Warwick, Coventry CV4 7 AL, UK
[7] University of Canterbury, Department of Physics and Astronomy, Private Bag 4800, Christchurch 8020, New Zealand
[8] Korea Astronomy and Space Science Institute, Daejon 34055, Republic of Korea
[9] University of Science and Technology, Korea (UST) Gajeong-ro, Yuseong-gu, Daejeon 34113, Republic of Korea
[10] Department of Physics, Chungbuk National University, Cheongju 28644, Republic of Korea
[11] Department of Particle Physics and Astrophysics, Weizmann Institute of Science, Rehovot 76100, Israel
[12] Center for Astrophysics | Harvard & Smithsonian, 60 Garden Street, Cambridge, MA 02138, USA
[13] Department of Astronomy and Tsinghua Centre for Astrophysics, Tsinghua University, Beijing 100084, People's Republic of China
[14] School of Space Research, Kyung Hee University, Yongin, Kyeonggi 17104, Republic of Korea

Abstract

Some low-mass planets are expected to be ejected from their parent planetary systems during early stages of planetary system formation. According to planet formation theories, such as the core accretion theory, typical masses of ejected planets should be between 0.3 and $1.0\,M_{\oplus}$. Although in practice such objects do not emit any light, they may be detected using gravitational microlensing via their light-bending gravity. Microlensing events due to terrestrial-mass rogue planets are expected to have extremely small angular Einstein radii ($\lesssim 1\,\mu$as) and extremely short timescales ($\lesssim 0.1$ day). Here, we present the discovery of the shortest-timescale microlensing event, OGLE-2016-BLG-1928, identified to date ($t_{\rm E} \approx 0.0288$ day = 41.5 minutes). Thanks to the detection of finite-source effects in the light curve of the event, we were able to measure the angular Einstein radius of the lens $\theta_{\rm E} = 0.842 \pm 0.064\,\mu$as, making the event the most extreme short-timescale microlens discovered to date. Depending on its unknown distance, the lens may be a Mars- to Earth-mass object, with the former possibility favored by the Gaia proper motion measurement of the source. The planet may be orbiting a star but we rule out the presence of stellar companions up to the projected distance of ~ 8.0 au from the planet. Our discovery demonstrates that terrestrial-mass free-floating planets can be detected and characterized using microlensing.

Unified Astronomy Thesaurus concepts: Gravitational microlensing (672); Gravitational microlensing exoplanet detection (2147); Finite-source photometric effect (2142); Free floating planets (549)

Supporting material: data behind figure

1. Introduction

Thousands of extrasolar planets have been discovered to date. Although many of the known exoplanets do not resemble those in our solar system, they have one thing in common—they all orbit a star. However, theories of planet formation and evolution predict the existence of free-floating (rogue) planets, gravitationally unattached to any star.

Exoplanets may be ejected from their parent planetary systems as a result of planet–planet scattering (Rasio & Ford 1996; Weidenschilling & Marzari 1996; Lin & Ida 1997; Chatterjee et al. 2008). It is estimated that at least 75% of systems

with giant planets must have experienced planet–planet scattering in the past (Raymond & Morbidelli 2020, and references therein). Dynamical interactions between giant planets inevitably lead to disruptions of orbits of inner smaller (rocky) planets (e.g., Veras & Armitage 2005; Matsumura et al. 2013; Carrera et al. 2016) and may lead to their ejection. In their population synthesis calculations (which are based on the core accretion theory of planet formation; Ida et al. 2013), Ma et al. (2016) found that typical masses of ejected planets are between 0.3 and $1.0\,M_{\oplus}$. According to their model, rogue planets are more likely to form around massive stars, which are in turn more likely to host giant planets. A similar

conclusion was reached by Barclay et al. (2017) who carried out N-body simulations of terrestrial planet formation around solar-type stars. They found that in the presence of giant planets in such systems, a large fraction of the protoplanetary material is ejected, partly in the form of Mars-mass bodies ($\sim$0.1–0.3 $M_\oplus$). Planets may also be liberated as a result of interactions in multiple-star systems (e.g., Kaib et al. 2013) and stellar clusters (e.g., Spurzem et al. 2009), stellar flybys (e.g., Malmberg et al. 2011), or the post-main-sequence evolution of the host star (e.g., Veras et al. 2011).

Dark compact objects, such as rogue planets, may be in principle detected in gravitational microlensing events—microlensing does not depend on the brightness of a lensing object. However, typical Einstein timescales of microlensing events due to sub-Earth-mass objects are extremely short:

$$t_{\rm E} = \frac{\theta_{\rm E}}{\mu_{\rm rel}} = 1.5 \, {\rm hr} \left(\frac{M}{0.3 \, M_\oplus}\right)^{1/2} \left(\frac{\pi_{\rm rel}}{0.1 \, {\rm mas}}\right)^{1/2} \left(\frac{\mu_{\rm rel}}{5 \, {\rm mas \, yr^{-1}}}\right)^{-1}, \quad (1)$$

rendering their detection difficult. (Here, $\theta_{\rm E}$ is the angular Einstein radius, $\mu_{\rm rel}$—relative lens-source proper motion, M—mass of the lens, and $\pi_{\rm rel}$—relative lens-source parallax.) If the radius of the source star is larger than the Einstein radius, the duration of microlensing events is extended thanks to finite-source effects (Gould 1994; Nemiroff & Wickramasinghe 1994; Witt & Mao 1994). For sub-Earth-mass lenses, finite-source effects become important if the angular radius of the source, θ_*, is of the order of the Einstein radius,

$$\theta_{\rm E} = 0.8 \, \mu{\rm as} \left(\frac{M}{0.3 \, M_\oplus}\right)^{1/2} \left(\frac{\pi_{\rm rel}}{0.1 \, {\rm mas}}\right)^{1/2}. \quad (2)$$

So far, only four short-timescale microlensing events exhibiting finite-source effects were identified (i.e., OGLE-2012-BLG-1323, $t_{\rm E} = 0.155 \pm 0.005$ day, $\theta_{\rm E} = 2.37 \pm 0.10$ μas; OGLE-2016-BLG-1540, $t_{\rm E} = 0.320 \pm 0.003$ day, $\theta_{\rm E} = 9.2 \pm 0.5$ μas; OGLE-2019-BLG-0551, $t_{\rm E} = 0.381 \pm 0.017$ day, $\theta_{\rm E} = 4.35 \pm 0.34$ μas; KMT-2019-BLG-2073, $t_{\rm E} = 0.267 \pm 0.026$ day, $\theta_{\rm E} = 4.77 \pm 0.19$ μas; Mróz et al. 2018, 2019, 2020; Kim et al. 2020). These events may be caused by unbound or wide-orbit ($\gtrsim$10 au) planets since microlensing observations alone are not able to rule out the presence of a distant stellar companion (as discussed in more detail by Mróz et al. 2020). These detections, together with short-timescale events found by Mróz et al. (2017), provide strong evidence for a large population of free-floating or wide-orbit planets in the Milky Way.

In this Letter, we present the discovery of the shortest-timescale microlensing event detected to date ($t_{\rm E} = 0.0288^{+0.0024}_{-0.0016}$ day, $\theta_{\rm E} = 0.842 \pm 0.064$ μas), which was likely caused by a Mars- to Earth-mass object.

2. Data

Microlensing event OGLE-2016-BLG-1928[15] occurred on 2016 June 18 (HJD$'$ = HJD $-$ 2,450,000 = 7557.8) on a

---

[15] This event was not detected in real-time by the OGLE Early Warning System (Udalski 2003). For consistency with previous works, we assigned it the name OGLE-2016-BLG-1928.
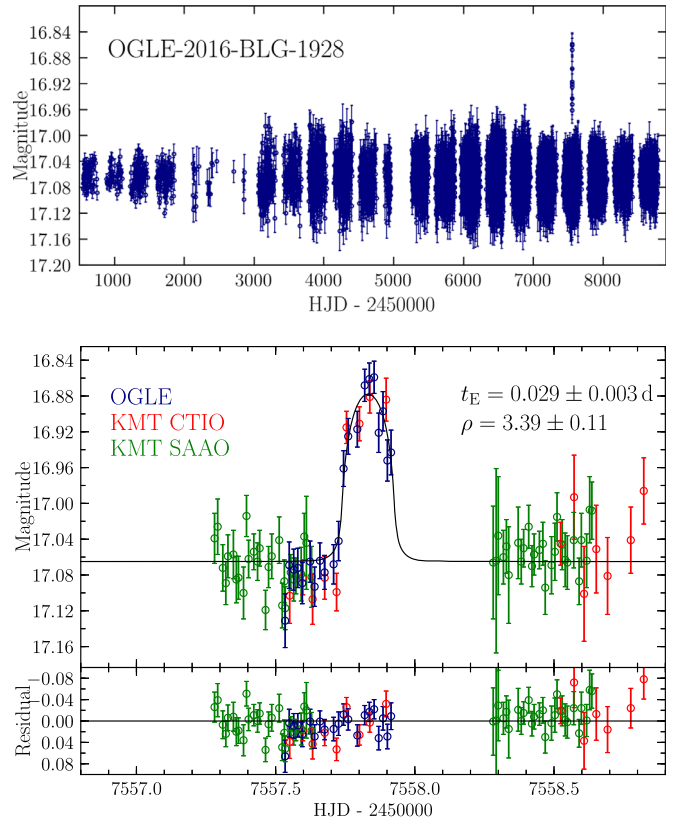

Figure 1. Upper panel: 23 yr long OGLE light curve of the microlensing event OGLE-2016-BLG-1928 reveals only one brightening that occurred on 2016 June 18 and lasted about 0.2 days. Lower panel: close-up of the magnified part of the light curve with the best-fitting microlensing model overplotted.

(The data used to create this figure are available.)

bright star ($I = 17.07$, $V - I = 1.91$) located at the equatorial coordinates of R.A. $= 18^{\rm h}01^{\rm m}31\overset{\rm s}{.}25$, decl. $= -29°07'46\overset{\prime\prime}{.}2$ (Galactic coordinates: $(l, b) = (1°596, -3°094)$). The event was found in data from the fourth phase of the Optical Gravitational Lensing Experiment (OGLE; Udalski et al. 2015) as part of the search for wide-separation planetary systems (R. Poleski et al. 2020, in preparation) but it has been observed by OGLE since 1997. The event was located near the area that was extensively monitored during the Campaign 9 of the K2 mission (Henderson et al. 2016)—both by K2 and numerous ground-based telescopes. However, only OGLE and one of the stations of the Korea Microlensing Telescope Network (KMTNet; Kim et al. 2016)—located in Cerro Tololo Interamerican Observatory (KMT CTIO)—captured the magnified part of the light curve (as shown in Figure 1). We used OGLE and KMT CTIO data in single-lens models. For binary-lens modeling, we included additional data from the KMTNet telescope in the Southern African Astronomical Observatory (KMT SAAO). The event was also observed six times during $7557.87 < {\rm HJD}' < 7558.17$ by the Microlensing Observations in Astrophysics (MOA) survey (Bond et al. 2001) under adverse weather conditions (poor seeing and clouds), which prevented us from extracting useful data. All analyzed data were collected in the I-band. The photometry was extracted using custom implementations of the difference image analysis (Alard & Lupton 1998) method by Woźniak (2000; OGLE) or Albrow et al. (2009; KMTNet).

Table 1
Microlensing Parameters for Best-fit Solutions

Point Lens			Binary Lens	
Parameter	Value ($f_s = 1$)	Value ($f_s \leqslant 1$)	Parameter	Value
t_0 (HJD′)	$7557.8332^{+0.0050}_{-0.0036}$	7557.8325 ± 0.0037	t_0 (HJD′)	7593.31 ± 0.74
t_E (days)	$0.0288^{+0.0024}_{-0.0016}$	0.0286 ± 0.0020	t_E (days)	$1.93^{+0.13}_{-0.17}$
u_0	$0.59^{+0.58}_{-0.42}$	$0.29^{+0.60}_{-0.29}$	u_0	$2.91^{+0.28}_{-0.39}$
ρ	$3.39^{+0.10}_{-0.11}$	$3.31^{+0.12}_{-0.25}$	ρ	0.0518 ± 0.0048
I_s	17.07 ± 0.05	$17.11^{+0.16}_{-0.05}$	s	$18.7^{+1.7}_{-1.1}$
f_s	1.0 (fixed)	$0.96^{+0.05}_{-0.13}$	q	$0.34^{+0.17}_{-0.10} \times 10^{-3}$
			α (deg)	188.8 ± 1.2

Note. HJD′ = HJD−2,450,000. $f_s = F_s/(F_s + F_b)$ is the dimensionless blending parameter.

3. Single-lens Models

The light curve of the event (Figure 1) can be well described by an extended-source point-lens model, which has four parameters: t_0 and u_0—time and projected separation during the closest approach between the lens and the center of the source, t_E—Einstein timescale, and $\rho = \theta_*/\theta_E$—which is the angular radius of the source θ_* expressed in θ_E units. The approximate values of these parameters can be estimated from the light curve without the need of sophisticated modeling (cf. Mróz et al. 2020): the maximum magnification A and duration Δt of the event are related to $\rho \approx \sqrt{2/(A - 1)} \approx 3.1$ and $t_E \approx \Delta t/2\rho = 0.03$ days. Indeed, in our best-fitting model we measure $\rho = 3.39^{+0.10}_{-0.11}$ and $t_E = 0.0288^{+0.0024}_{-0.0016}$ days (Table 1). Microlensing magnifications are computed using the method described by Bozza et al. (2018), we assume a linear limb-darkening law with $\Gamma = 0.46$ (as appropriate for the effective temperature of the source of 5000 ± 200 K, see Section 5; Claret & Bloemen 2011). The best-fitting parameters and their uncertainties are estimated using the Markov Chain Monte Carlo sampler of Foreman-Mackey et al. (2013).

During the modeling we fix the value of the dimensionless blending parameter $f_s = 1$, that is, we assume that the entire flux comes from the source star. Usually, for every data set, there are two additional parameters that describe the source flux F_s and unmagnified blend flux F_b. We define $f_s = F_s/(F_s + F_b)$. When both F_s and F_b were allowed to vary, the best-fitting solutions had large negative blending flux ($f_s \gtrsim 3$), such solutions are unphysical. The best-fitting model with $f_s = 1$ is disfavored by only $\Delta\chi^2 = 4.8$, which may be due to a statistical fluctuation or low-level systematics in the data. As demonstrated by Mróz et al. (2020), blending does not influence the inferred value of θ_E provided that the blend and source have similar colors. Thus, in our final models, we kept $F_b = 0$ (that is, $f_s = 1$) constant, but we also added in quadrature 0.05 mag to the uncertainty of the source brightness. For comparison, the best-fit parameters for the free-blending fit (assuming $f_s \leqslant 1$) are also presented in Table 1. Blending may affect the characterization of the lens only if the blend and source have significantly different colors, as discussed in detail by Mróz et al. (2020) and Kim et al. (2020).

4. Binary-lens Models

The light curve of OGLE-2016-BLG-1928 shows a clear signal from a low-mass planet, but it does not show an obvious signal from a host of the planet. To search for a host, we fitted a binary-lens model to the data. The binary-lens model has three parameters more than the single-lens model and these are: s—the projected separation between the planet and host expressed in Einstein radii (of the total mass of the system), q—planet to host mass ratio, and α—angle between the binary axis and the source trajectory. We started the search for binary-lens models by defining t_0, u_0, and t_E relative to the planet (Han 2006; Mróz et al. 2020), because then the values of the four parameters (t_0, u_0, t_E, ρ) are well constrained by the light curve. In order to speed-up calculations, we neglected limb-darkening of the source. The magnification of the finite-source binary-lens model was evaluated using the method presented by Bozza (2010) and Bozza et al. (2018). The fitting was done using the MulensModel code by Poleski & Yee (2019). After these initial fits converged, we reran the fits in standard parameterization (t_0, u_0 defined relative to the center of mass, and t_E relative to the total mass of the system) and including limb-darkening of the source.

The parameters of the best-fit binary-lens model are presented in Table 1. When compared to the single-lens model, the χ^2 improves by 44.2. The main difference between single-lens and binary-lens models is the presence of a low-amplitude bump at HJD′ ≈ 7593. The χ^2 improvement, however, comes mostly from one observatory (OGLE) from one night and the KMT data from that night do not corroborate the signal (Figure 2). The bump could have an origin other than the microlensing of planet host: it could be produced by low-level fluctuations in the light curve (either of instrumental origin, intrinsic variability, or a combination of both). We cannot judge the reliability of the binary-lens fit using the Bayesian approach because we cannot present a meaningful prior on such a binary-lens model. Instead, we decided to check $\Delta\chi^2$ relative to a constant brightness model and determine whether similar bumps are present in other seasons of the OGLE-IV data. We fitted point-source point-lens models to each of the observing seasons 2010–2015 and 2017–2019. For each season (i), we calculated χ^2 difference between the above fit and a model of constant brightness ($\Delta\chi_i^2$). In order to compare these values with the bump in 2016 we normalized them by the number of epochs in the given season: $\Delta\chi_i^2 N_{2016}/N_i$, where $N_{2016} = 1621$. The results of these calculations are presented in Table 2. The $\Delta\chi_{2016}^2$ between point-lens and binary-lens models for 2016 data is 32.5 when only OGLE data are considered. We see that in four out of nine other seasons the $\Delta\chi_i^2 N_{2016}/N_i$ is higher than 32.5, hence, the probability that the bump detected in binary-lens analysis is just the manifestation of low-level fluctuations as seen in other seasons is 4/9 = 44%.
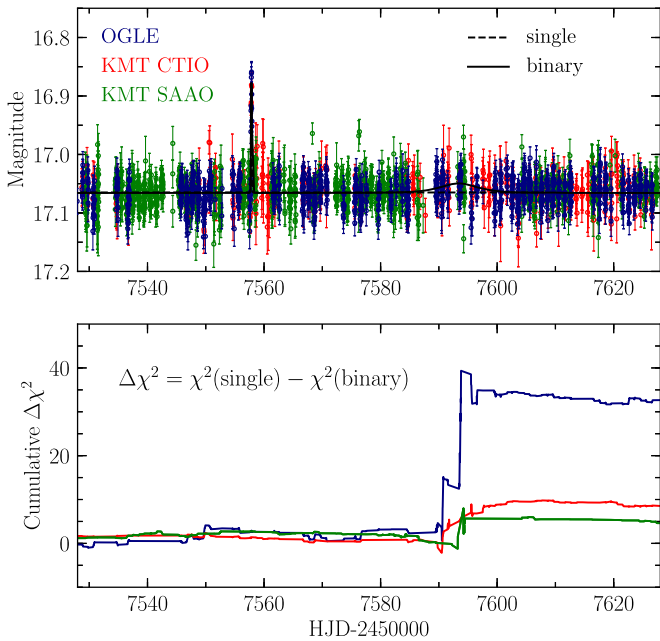
Figure 2. Upper panel: comparison between the single- (dashed line) and binary-lens (solid line) models. Lower panel: cumulative distribution of $\Delta\chi^2$ between these models.

Table 2
Statistics of Trends Seen in OGLE Data in Seasons 2010–2015 and 2017–2019

Year	N_i	$\Delta\chi_i^2 N_{2016}/N_i$
2010	651	45.2
2011	813	26.2
2012	2317	51.7
2013	2309	41.7
2014	2277	13.9
2015	2170	10.2
2017	707	68.1
2018	724	30.8
2019	824	16.7

Moreover, the parameters of the binary-lens model point to a very unusual system, suggesting that the bump in the light curve is not due to microlensing. The Einstein timescale of 1.9 days is extremely short and suggests that the host has a mass of a few Jupiter masses, and hence may be a planet as well. Additionally, the projected separation $s \approx 19$ is almost four times larger than the widest separation microlensing planet currently known (OGLE-2008-BLG-092, $s = 5.3$; Poleski et al. 2014).

Since there is no strong evidence for a host star from the microlensing light curve, we use the method of Mróz et al. (2018, 2019) to estimate lower limits on the projected star–planet separation of a putative host star. We consider a $0.3\,M_\odot$ host located either in the Galactic disk ($\pi_{\rm rel} = 0.1$ mas) or in the bulge ($\pi_{\rm rel} = 0.016$ mas), which correspond to $\theta_{\rm E,host} = 0.49$ mas or 0.20 mas, respectively. Then, we simulate synthetic OGLE light curves (spanning from 2010 March 5 through 2019 October 30) assuming $q = (\theta_{\rm E}/\theta_{\rm E,host})^2$, $1 \leqslant s \leqslant 10$, and $0 \leqslant \alpha \leqslant 2\pi$. For each pair of (q,s) we calculate the fraction of light curves that show signatures of the host star. We find a 90% lower limit on the projected host separation of 3.6 Einstein radii for the lens located in the disk ($\pi_{\rm rel} = 0.1$ mas) and 3.3 Einstein radii for the bulge
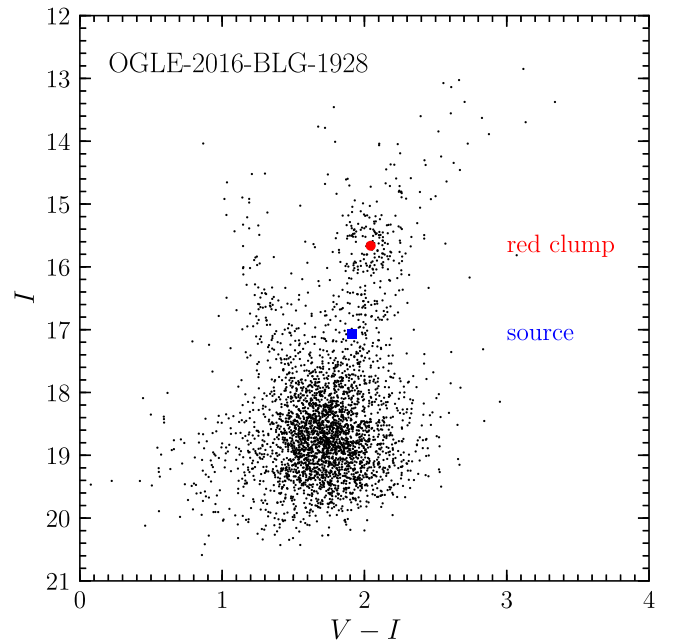

Figure 3. Color–magnitude diagram of stars located within $2' \times 2'$ of the microlensing event OGLE-2016-BLG-1928.

lens ($\pi_{\rm rel} = 0.016$ mas). These limits translate to 8.0 au and 4.6 au, respectively.

We also searched for binary-lens solutions in which the observed brightening is due to a cusp crossing. We did a grid search with $-2 \leqslant \log q \leqslant 0$ and $0.2 \leqslant s \leqslant 3$. We considered only trajectories that cross the caustic twice during the night of $\mathrm{HJD}' = 7557$ and parameterized the models using the Cassan (2008) approach. In the best-fitting model ($t_{\rm E} = 0.020$ day, $\rho = 2.4$, $s = 4.4$, $q = 0.86$), the source envelops the caustics. Although this model is better by $\Delta\chi^2 = 10.0$ than the best single-lens model, we find it unlikely (this is essentially the same model but with an extra body). We found $t_{\rm E} < 0.05$ days for all binary-lens models in the grid search.

5. Physical Parameters

The light curve of the event OGLE-2016-BLG-1928 (Figure 1) exhibits prominent finite-source effects that enable us to measure the angular Einstein radius of the lens provided that the angular radius of the source star is known: $\theta_{\rm E} = \theta_*/\rho$. We use the color–surface brightness relation of Pietrzyński et al. (2019) to calculate θ_*. To determine the dereddened color $(V - I)_{\rm s,0}$ and brightness $I_{\rm s,0}$ of the source, we use the standard method of Yoo et al. (2004). We measure that the source is $\Delta(V - I) = -0.13 \pm 0.02$ bluer and $\Delta I = 1.40 \pm 0.09$ fainter than the red clump centroid in the color–magnitude diagram (Figure 3). Because the dereddened color ($(V - I)_{\rm RC,0} = 1.06$) and brightness ($I_{\rm RC,0} = 14.38$) of red clump stars in this direction are known (Bensby et al. 2011; Nataf et al. 2013), we measure $(V - I)_{\rm s,0} = 0.93 \pm 0.02$ and $I_{\rm s,0} = 15.78 \pm 0.09$. Subsequently, we determine $(V - K)_{\rm s,0} = 2.12 \pm 0.07$ using the color–color relations of Bessell & Brett (1988) and $\theta_* = 2.85 \pm 0.20\ \mu$as using the color–surface brightness relation of Pietrzyński et al. (2019).

The calculation above is based on two assumptions. First, we assume that the source star and red clump stars are reddened by the same amount. Because the Gaia proper motion of the source relative to the mean proper motion of red clump stars is only 0.18 mas yr^{-1} (Gaia Collaboration et al. 2018) (Figure 4), the
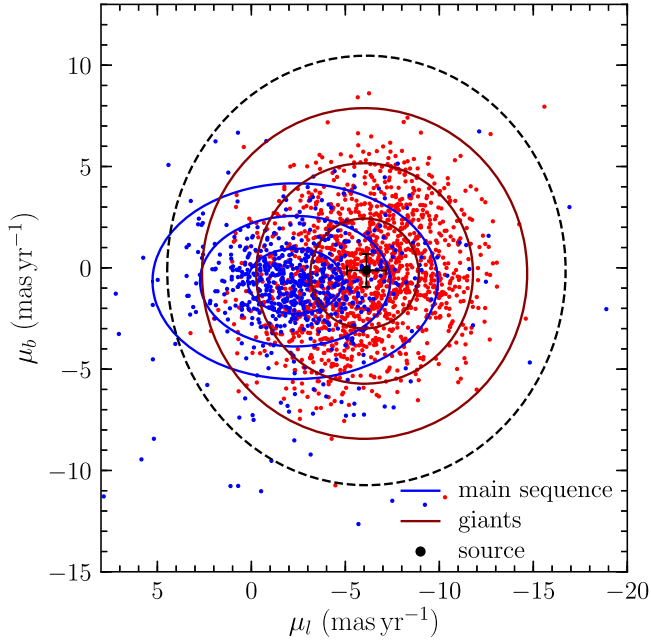
Figure 4. Gaia proper motions of stars located within 5′ of the event (Gaia Collaboration et al. 2018). Red giant stars (representing the Galactic bulge population) are marked by red dots, while main-sequence stars (Galactic disk population) are marked by blue dots. Solid contours mark (1, 2, 3)σ error ellipses based on the scatter in the distribution. The proper motion of the source and its position on the color–magnitude diagram are consistent with those of Galactic bulge stars. The relative lens-source proper motion is $\mu_{\rm rel} = 10.6 \pm 1.0$ mas yr^{-1}, so the lens should be located on a dashed circle.

source is likely located in the Galactic bulge and so the first assumption holds true. Second, we assume that the color of the source is equal to that of the baseline object. Neither OGLE nor KMTNet observed the magnified part of the event in the V-band filter, which prevents us from directly calculating the color of the source. Because the best-fitting model evinces no evidence for blended light from unresolved ambient stars, our best estimate of the color of the source is the color of the baseline object.

Having the angular radius of the source star measured, we can calculate the angular Einstein radius:

$$\theta_{\rm E} = \frac{\theta_*}{\rho} = 0.842 \pm 0.064 \ \mu{\rm as} \quad (3)$$

and the relative lens-source proper motion (in the geocentric frame):

$$\mu_{\rm rel} = \frac{\theta_{\rm E}}{t_{\rm E}} = 10.6 \pm 1.0 \ {\rm mas \ yr}^{-1}. \quad (4)$$

6. Discussion

With the Einstein timescale of $t_{\rm E} = 0.0288^{+0.0024}_{-0.0016}$ days $= 41.5^{+3.5}_{-2.3}$ minutes and the angular Einstein radius of $\theta_{\rm E} = 0.842 \pm 0.064 \ \mu{\rm as}$, OGLE-2016-BLG-1928 is the most extreme short-timescale microlensing event discovered to date. The mass of the lens cannot be determined because the relative lens-source parallax cannot be measured:

$$M = \frac{\theta_{\rm E}^2}{\kappa \pi_{\rm rel}}, \quad (5)$$

Table 3
Physical Parameters for the Source and Lens for Point Lens ($f_{\rm s} = 1.0$ Solution)

Parameter	Value
Source:	
$I_{\rm s,0}$	15.78 ± 0.08
$(V - I)_{\rm s,0}$	0.93 ± 0.02
$(V - K)_{\rm s,0}$	2.12 ± 0.07
$T_{\rm eff}$ (K)	5000 ± 200
Γ (limb-darkening, I band)	0.46
θ_* (μas)	2.85 ± 0.20
μ_l (mas yr^{-1})	-6.12 ± 1.03
μ_b (mas yr^{-1})	-0.13 ± 0.81
Lens:	
$\theta_{\rm E}$ (μas)	0.842 ± 0.064
$\mu_{\rm rel}$ (mas yr^{-1})	10.6 ± 1.0

where $\kappa = 8.144$ mas $M_\odot^{-1}$. If the lens is located in the Galactic disk ($\pi_{\rm rel} \approx 0.1$ mas), then $M \approx 0.3 \ M_\oplus$ (which is approximately three Mars masses). The lens located in the Galactic bulge (typically $\pi_{\rm rel} \approx 0.016$ mas) would be more massive ($M \approx 2 \ M_\oplus$).

The Gaia proper motion of the source (Table 3) favors the interpretation that the lens is located in the Galactic disk, so the lens should be a sub-Earth-mass object. The proper motion of the source is consistent with that of red clump stars (Figure 4), and the relative lens-source proper motion is $\mu_{\rm rel} = 10.6 \pm 1.0$ mas yr^{-1}. In order to have this relative proper motion, the lens should lie in the region around a dashed circle marked in Figure 4 and there are virtually no Galactic bulge stars in this region (while there exist some disk stars). To quantify this, we can directly measure the proper motion distribution of Galactic bulge stars using Gaia data (Figure 4). This distribution can be approximated as a Gaussian with dispersions of 2.884 ± 0.052 and 2.720 ± 0.049 mas yr^{-1} in the l and b directions, respectively. Thus the probability that the proper motion of the lens is consistent with that of bulge stars is smaller than 2×10^{-4}.

The lens in OGLE-2016-BLG-1928 is likely a sub-Earth-mass object, one of the lowest-mass objects ever found by microlensing. As in the case of other short-timescale microlensing events (Sumi et al. 2011; Mróz et al. 2018, 2019, 2020; Kim et al. 2020), we cannot rule out the presence of a distant stellar companion. We conducted an extensive search for possible binary-lens models—we found that the best-fitting binary-lens model is preferred by $\Delta\chi^2 = 44.2$ over the single-lens model. Although this appears to be statistically significant, we found that the source exhibits low-level fluctuations, which may mimic a microlensing signal from a host star. Thus, we do not find any significant evidence for the host star up to the projected distance of 8.0 au from the planet (assuming $\pi_{\rm rel} = 0.1$ mas).

The properties of OGLE-2016-BLG-1928 place it at the edge of current limits of detecting short-timescale microlensing events and highlight the challenges that will be faced by future surveys for extremely short-timescale events (for example, by the Nancy Grace Roman Space Telescope, formerly known as WFIRST, Johnson et al. 2020). Despite the fact that the event was located in high-cadence survey fields, only 15 data points were magnified (11 from OGLE and 4 from KMTNet), rendering the event difficult to detect. In particular, the declining part of the light curve is not fully covered with observations (Figure 1).

This raises the question of whether the observed light curve is due to a genuine microlensing event in the first place. The source star is located in the red giant branch in the color–magnitude diagram (Figure 3), and some giants are known to produce stellar flares (e.g., van Doorsselaere et al. 2017; Iwanek et al. 2019). However, the properties of the event (its duration, amplitude, and light-curve shape) do not match those of flaring stars. For example, Balona (2015) compiled an atlas of stellar flares observed by the Kepler satellite in short-cadence mode. They found that 97.8% of stellar flares are shorter than 0.2 days and that the light-curve shapes and amplitudes of the remaining 2.2% do not match those of OGLE-2016-BLG-1928. We also note that the event has been observed by OGLE since 1997 and there is no evidence for other flares (nor periodic variability due to star spots) in the archival data, suggesting the object is unlikely to be a flaring star.

Another issue resulting from the short duration of the event is the lack of color measurements while the source is magnified. According to Mróz et al. (2020), in microlensing events exhibiting strong finite-source effects, the angular Einstein radius depends on the surface brightness of the source, which make color measurements critical for determining θ_E. In the present case, we assumed that the source color is equal to the color of the baseline object, which is motivated by the lack of evidence for the blended light in the best-fitting models. This issue may become more important for the Roman telescope, which is being designed to carry out observations in *W146* filter with a 15 minute cadence and in *Z087* filter with a 12 hr cadence. Johnson et al. (2020) estimate that only approximately 10% of short-timescale events due to 1 $M_\oplus$ lenses would have a color measurement. We thus advocate that the frequency of *Z087* filter observations should be increased.

The discovery of OGLE-2016-BLG-1928 demonstrates that current microlensing surveys are capable of finding extremely short-timescale events. Although the mass of the lens cannot be unambiguously measured, properties of the event are consistent with the lens being a sub-Earth-mass object with no stellar companion up to the projected distance of ~8 au from the planet. Thus, the lens is one of the best candidates for a terrestrial-mass rogue planet detected to date. This population of low-mass free-floating (or wide-orbit) planets may be further explored by the upcoming microlensing experiments.

ORCID iDs

Przemek Mróz ⦿ https://orcid.org/0000-0001-7016-1692
Radosław Poleski ⦿ https://orcid.org/0000-0002-9245-6368
Andrzej Udalski ⦿ https://orcid.org/0000-0001-5207-5619
Michał K. Szymański ⦿ https://orcid.org/0000-0002-0548-8995
Igor Soszyński ⦿ https://orcid.org/0000-0002-7777-0842
Paweł Pietrukowicz ⦿ https://orcid.org/0000-0002-2339-5899
Szymon Kozłowski ⦿ https://orcid.org/0000-0003-4084-880X
Jan Skowron ⦿ https://orcid.org/0000-0002-2335-1730
Krzysztof Ulaczyk ⦿ https://orcid.org/0000-0001-6364-408X
Michael D. Albrow ⦿ https://orcid.org/0000-0003-3316-4012
Sun-Ju Chung ⦿ https://orcid.org/0000-0001-6285-4528
Cheongho Han ⦿ https://orcid.org/0000-0002-2641-9964
Kyu-Ha Hwang ⦿ https://orcid.org/0000-0002-9241-4117
Yoon-Hyun Ryu ⦿ https://orcid.org/0000-0001-9823-2907
In-Gu Shin ⦿ https://orcid.org/0000-0002-4355-9838
Yossi Shvartzvald ⦿ https://orcid.org/0000-0003-1525-5041
Jennifer C. Yee ⦿ https://orcid.org/0000-0001-9481-7123
Weicheng Zang ⦿ https://orcid.org/0000-0001-6000-3463
Richard W. Pogge ⦿ https://orcid.org/0000-0003-1435-3053

References

Alard, C., & Lupton, R. H. 1998, ApJ, 503, 325
Albrow, M. D., Horne, K., Bramich, D. M., et al. 2009, MNRAS, 397, 2099
Balona, L. A. 2015, MNRAS, 447, 2714
Barclay, T., Quintana, E. V., Raymond, S. N., & Penny, M. T. 2017, ApJ, 841, 86
Bensby, T., Adén, D., Meléndez, J., et al. 2011, A&A, 533, A134
Bessell, M. S., & Brett, J. M. 1988, PASP, 100, 1134
Bond, I. A., Abe, F., Dodd, R. J., et al. 2001, MNRAS, 327, 868
Bozza, V. 2010, MNRAS, 408, 2188
Bozza, V., Bachelet, E., Bartolić, F., et al. 2018, MNRAS, 479, 5157
Carrera, D., Davies, M. B., & Johansen, A. 2016, MNRAS, 463, 3226
Cassan, A. 2008, A&A, 491, 587
Chatterjee, S., Ford, E. B., Matsumura, S., & Rasio, F. A. 2008, ApJ, 686, 580
Claret, A., & Bloemen, S. 2011, A&A, 529, A75
Foreman-Mackey, D., Hogg, D. W., Lang, D., & Goodman, J. 2013, PASP, 125, 306
Gaia Collaboration, Brown, A. G. A., Vallenari, A., et al. 2018, A&A, 616, A1
Gould, A. 1994, ApJL, 421, L71
Han, C. 2006, ApJ, 638, 1080
Henderson, C. B., Poleski, R., Penny, M., et al. 2016, PASP, 128, 124401
Ida, S., Lin, D. N. C., & Nagasawa, M. 2013, ApJ, 775, 42
Iwanek, P., Soszyński, I., Skowron, J., et al. 2019, ApJ, 879, 114
Johnson, S. A., Penny, M., Gaudi, B. S., et al. 2020, AJ, 160, 123
Kaib, N. A., Raymond, S. N., & Duncan, M. 2013, Natur, 493, 381
Kim, H.-W., Hwang, K.-H., Gould, A., et al. 2020, arXiv:2007.06870
Kim, S.-L., Lee, C.-U., Park, B.-G., et al. 2016, JKAS, 49, 37
Lin, D. N. C., & Ida, S. 1997, ApJ, 477, 781
Ma, S., Mao, S., Ida, S., Zhu, W., & Lin, D. N. C. 2016, MNRAS, 461, L107
Malmberg, D., Davies, M. B., & Heggie, D. C. 2011, MNRAS, 411, 859
Matsumura, S., Ida, S., & Nagasawa, M. 2013, ApJ, 767, 129
Mróz, P., Poleski, R., Han, C., et al. 2020, AJ, 159, 262
Mróz, P., Ryu, Y.-H., Skowron, J., et al. 2018, AJ, 155, 121
Mróz, P., Udalski, A., Bennett, D. P., et al. 2019, A&A, 622, A201
Mróz, P., Udalski, A., Skowron, J., et al. 2017, Natur, 548, 183
Nataf, D. M., Gould, A., Fouqué, P., et al. 2013, ApJ, 769, 88
Nemiroff, R. J., & Wickramasinghe, W. A. D. T. 1994, ApJL, 424, L21
Pietrzyński, G., Graczyk, D., Gallenne, A., et al. 2019, Natur, 567, 200
Poleski, R., Skowron, J., Udalski, A., et al. 2014, ApJ, 795, 42
Poleski, R., & Yee, J. C. 2019, A&C, 26, 35
Rasio, F. A., & Ford, E. B. 1996, Sci, 274, 954
Raymond, S. N., & Morbidelli, A. 2020, arXiv:2002.05756
Spurzem, R., Giersz, M., Heggie, D. C., & Lin, D. N. C. 2009, ApJ, 697, 458
Sumi, T., Kamiya, K., Bennett, D. P., et al. 2011, Natur, 473, 349
Udalski, A. 2003, AcA, 53, 291
Udalski, A., Szymański, M. K., & Szymański, G. 2015, AcA, 65, 1
van Doorsselaere, T., Shariati, H., & Debosscher, J. 2017, ApJS, 232, 26
Veras, D., & Armitage, P. J. 2005, ApJL, 620, L111
Veras, D., Wyatt, M. C., Mustill, A. J., Bonsor, A., & Eldridge, J. J. 2011, MNRAS, 417, 2104
Weidenschilling, S. J., & Marzari, F. 1996, Natur, 384, 619
Witt, H. J., & Mao, S. 1994, ApJ, 430, 505
Woźniak, P. R. 2000, AcA, 50, 421
Yoo, J., DePoy, D. L., Gal-Yam, A., et al. 2004, ApJ, 603, 139